Physica **44** (1969) 177–205 © *North-Holland Publishing Co., Amsterdam*

COLLISIONS OF Ar^+ IONS WITH SURFACE Cu ATOMS AND CHARGE EXCHANGE OF SCATTERED IONS NEAR THE METAL SURFACE

W. F. VAN DER WEG and D. J. BIERMAN

FOM-Instituut voor Atoom- en Molecuulfysica, Amsterdam, Nederland

Received 11 February 1969

Synopsis

Absolute intensities of scattered projectile and recoil ions resulting from large-angle collisions of 60 and 90 keV Ar^+ ions in a (100) surface of a solid Cu target are presented. These intensities are studied as a function of scattering angle and also as a function of the angle between the direction of emerging ions and the surface.

A model is proposed which interrelates the observed ion yields in the cases of ion-surface atom scattering and ion-gas atom scattering. This model describes the collision of an ion with a surface atom in two phases. The first phase essentially neglects any interaction of the two collision partners with the metal surface and therefore is exactly the same as the model to describe ion-free atom collisions.

The second phase starts after the moment that ion formation has taken place and consists of a continuous interaction of the scattered ions with the surface on their path to the analyzer. The interaction is assumed to be charge exchange of the ions by capture of metal electrons. These processes are found to have rates of about 10^{15}/s depending on charge state and metal-ion distance.

1. *Introduction.* It is known that some aspects of two-body atomic collisions in the keV range can be studied, using metal surface atoms as a target[1,2]). The kinetic energies of the scattered particles and the inelastic energy dissipated during the collision are the same for a gas target and the corresponding solid target[3]).

Large differences, however, occur in the charge states of the scattered particles, depending on the state of the target[4]). The charge of noble gas particles scattered from a solid has always been found to be lower than the charge of scattering products resulting from a collision in a gas.

The aim of this paper is to describe the nature of this difference.

We apply a model which describes the scattering process on a solid surface in two phases:

1) The collision of a projectile with a target atom takes place without disturbance by the surrounding metal atoms. In fact, we treat the first stage of the collision as a collision in a gas.

2) After the collision, when ion formation has taken place, interaction of these highly-charged ions takes place with the solid, resulting in charge changing processes, which decrease the ionic charges.

We take Auger-like processes, in which ions formed by the violent collision and metal electrons participate, as the mechanism responsible for the charge changing. This model for the charge transfer process is an extension of the mechanism for potential electron ejection[5]).

Experimentally we study the charge changing process in two ways. The first method is comparison of P_n (fraction of n times charged ions) *vs* scattering angle curves measured with a gaseous and a solid target. This method will lead to an estimation of the transition probability for Auger processes near a solid surface. The second means of obtaining information is a variation of the time of flight of ions near the surface, thus varying the probability for electron transitions. These measurements reveal strong influence of neighbour atoms of the scattering center. The effects can be explained in terms of enhanced transition probability for Auger processes near surface atoms.

This description of collisions of projectile ions with surface atoms stresses further the analogy with collisions in a gas. To a certain degree, the metal may be considered as a dense gas of atoms, with which the primary ions collide. Interaction of scattering products with other target atoms changes their charge subsequently.

2. *Experimental.* 2.1. Apparatus. The measurements were performed in a scattering chamber and analyzing system, already described elsewhere in detail[6]). An Ar^+ ion beam with energy between 30 and 90 keV enters a scattering chamber through collimating slits a and b and hits the target (fig. 1).

A spot of size $1 \times 2\ mm^2$ is bombarded on the target. This area acts as

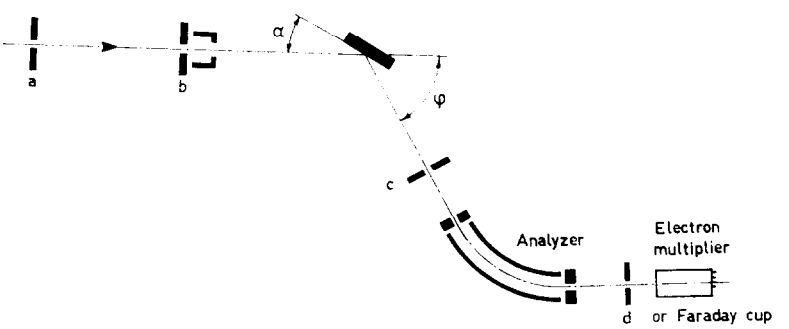

Fig. 1. Schematic view of the apparatus.
The incoming beam is collimated by the apertures a and b; ions scattered from the target through the aperture c are analyzed and detected.

a source of scattered particles which enter an electrostatic energy analyzer through a circular diaphragm c with a diameter of 1 mm, located at 185 mm from the scattering center. Between the target and the slit through which the primary beam enters an aperture was mounted, which was kept at a potential of −60 C, in order to prevent secondary electrons formed at the beam defining slit b to reach the target. The target itself is kept at +30 V to trap secondary electrons. Measurement of the beam current on the target while increasing the target voltage, did not show a variation, so we can assume all electrons to be suppressed. Acceleration of scattered ions by the target voltage influences the position of the scattered ion peaks in the energy spectrum, but not their intensity in which we are interested.

2.2. Surface condition of the target. The pressure in the scattering chamber is 10^{-6} Torr, it is maintained by a baffled mercury diffusion pump. The beam current density is in the order of 2 $\mu A/mm^2$. The sputtering rate of 30–90 keV Ar^+ on Cu is high enough[7,8] to maintain a clean surface (degree of covering less than 5%) with these experimental conditions.

We have two experimental verifications of this conclusion. Firstly, in the energy spectrum of scattered particles one never observes peaks of primary ions scattered from impurities on the surface, or peaks of scattered surface impurities. Also no peaks resulting from scattering by built-in Ar atoms have been found. It is remarkable that all ions which are shot into the target give no contribution to the energy spectrum of scattered particles. This fact can be explained by the observations of Nelson on the fate of the gas injected into solids by ion bombardment[9]). These injected atoms cluster together and form bubbles, which explode under or near the surface. So no beam atoms are found at surface lattice positions. A second indication of the cleaning of the target by the primary beam is the time behaviour of the intensity of the ion peaks in the energy spectrum. The first few minutes after the beginning of the ion bombardment the scattered ion intensities decrease, reaching a constant value after a few minutes, remaining at this value during the whole course of the experiment. We ascribe the initial decrease in intensity to cleaning of the surface by the sputtering process. It is known that surface contamination increases the number of emitted ions for the case of noble gas ions on metals[10]). We used 99.999% pure Cu single crystals with surfaces having a (100), (110) or a (111) orientation. The crystals are mechanically polished first and then electropolished on a Disa Electropol (Struers, Copenhagen) before mounting in the targetholder. It is observed during the experiments that the crystals maintain their single crystalline structure during ion bombardment, although the primary ions certainly induce surface roughness which can be observed by the eye after bombardment during an hour with 2 $\mu A/mm^2$ current density. It can be concluded that the annealing of radiation damage takes place in the time interval between the arrival of two successive beam ions.

The target holder permits the crystal to be rotated around 3 perpendicular directions. Two rotations can be performed with the crystal in vacuo.

Scattered particles are analyzed by a 72° cylindrical electrostatic analyzer and measured with a Bendix electron multiplier (type M 306) connected to a General Radio electrometer (type 1230 A). Also a Faraday cup could be mounted in the place of the multiplier, in which case the currents were measured with a vibrating reed electrometer (EIL). The electrometer signal is recorded by an XY recorder, which receives its X signal by the analyzer voltage divider.

3. *Measurements of scattered ion intensities.* 3.1. Principle of the measurement. Our primary aim is to determine absolute intensities of ions with different charge resulting from bi-particle collisions on the metal surface. Therefore we use a single crystal as a target, and direct the primary beam along an open (low index) crystal direction. Under these circumstances, effects from multiple collisions and deeper layers are minimized.

The experimental procedure to determine scattered ion intensities is the following. For a fixed scattering angle an energy over charge spectrum of scattered particles is recorded. In it, several peaks of Ar and Cu ions with different charges, resulting from single collisions of Ar^+ with surface Cu atoms are present[2]). The background is formed by multiply scattered particles. In case of absolute current measurements with the Faraday cup the total number of particles per second in a peak is given by

$$N = \int_{\text{peak}} N(E)\,\mathrm{d}E = \int \frac{I(E)\,\mathrm{d}E}{\Delta E\, ne}; \tag{1}$$

$N(E)$ = number of secondary ions per second per unit energy as a function of the energy E;
$I(E)$ = secondary ion current at energy E;
ne = charge of the ions;
ΔE = bandwidth of the analyzer.

In our analyzer the bandwidth is related to the energy like $\Delta E/E = \frac{3}{250}$. So for a narrow peak with mean energy $\bar{E}$ we can take E constant over the peak, in which case $\Delta E = \frac{3}{250}\bar{E}$ holds.

The total number of scattered ions of charge number n per incoming ion can be given

$$\frac{N}{N_0} = \frac{250S}{3I_0 n\bar{E}}, \tag{2}$$

in which $I_0 = N_0 e$ = primary current, and

$$S = \int_{\text{peak}} I(E)\,\mathrm{d}E = \text{peak area}.$$

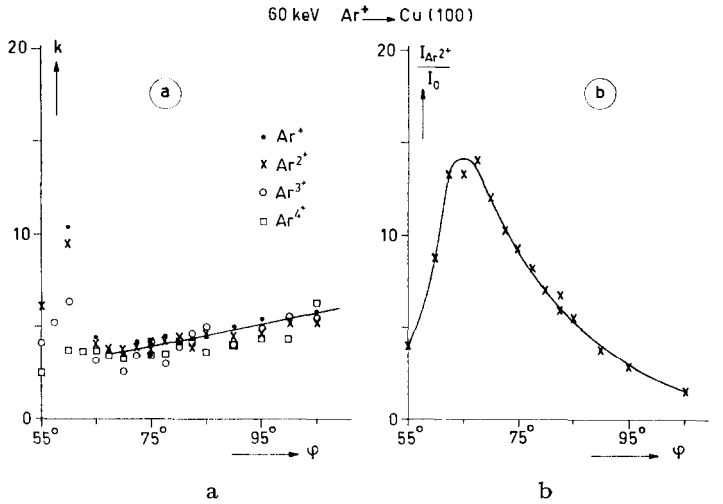

a b

Fig. 2a. The mean peak width k as a function of scattering angle in arbitrary units. For large φ, k is due to the finite solid angle accepted by the analyzer and the spread in inelastic energy loss. Below $\varphi = 60°$ double scattering effects cause deviations. 2b. Intensity of the Ar^{2+} peak normalized on beam current as measured with the Bendix multiplier.

We write (2) like

$$\frac{N}{N_0} = \frac{I}{nI_0} \cdot \frac{250}{3} \cdot \frac{S}{I\bar{E}}. \tag{2a}$$

Here I/nI_0 is the secondary-ion current at the top of the peak per unit of primary-ion current and $k = \frac{250}{3} S/I\bar{E}$ is the area of a peak divided by the current at the top of the peak and divided by the analyzer bandwidth, in other words it is the mean-width of the peak expressed in units of analyzer bandwidth. We separate formula (2) in this way because the factor k is a constant for a certain scattering angle, it does not depend on the particular ion.

Combination of measurements of k for different ions enables us to determine k with larger accuracy. This mean width k is shown in fig. 2a as a function of scattering angle φ, for the case of 60 keV Ar^+ on a (100) surface of Cu, with beam incidence along a [110] direction, making an angle of 45° with the surface.

One observes that for scattering angles $\varphi > 65°$ the peakwidths are independent of charge. Below 65° large deviations occur. The peakwidths increase, which effect is more pronounced for the lower charges. We ascribe it to double scattering effects.

3.2. Double collisions effects. For certain regions of scattering angles the conditions for a single collision description of the experiment are no

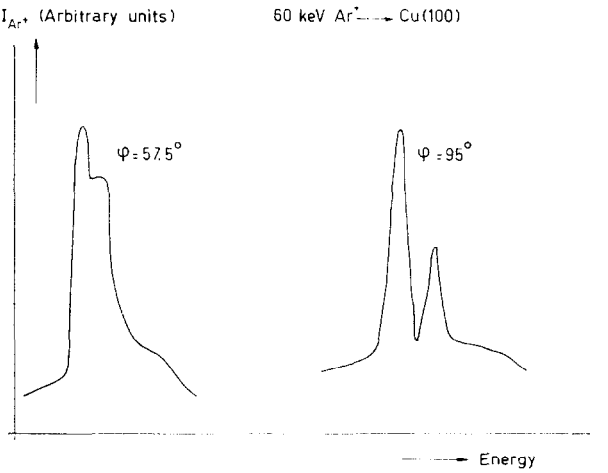

Fig. 3. The change of peak form of scattered Ar^+ due to double scattering ($\varphi = 57.5°$), compared with the undisturbed case ($\varphi = 95°$). For all scattering angles Ar peaks are double, because of scattering from the two Cu isotopes ^{63}Cu and ^{65}Cu.

longer fulfilled. This occurs when scattered particles leave the surface grazingly. Then the scattered particles undergo weak collisions with neighbours of the scattering centre. Particles scattered in this way into a certain scattering angle φ will retain more energy than when scattered in the same direction by a single collision. This should result in a shift of the peak in the energy spectrum. Experimentally, however, we find an appreciable broadening of the peak. There are still particles found with an energy which is characteristic for single collisions evidently originating from a scattering centre without a neighbour. This indicates that there are in a surface under ion bombardment many un-occupied lattice positions. Evidences for monoatomic ridges and vacancies in a surface after ion bombardment has also been provided by LEED[14,15]. In fig. 3 we see two examples of peaks: one for a large scattering angle where no particles are observed with energies other than those which we can expect from a single collision.

In the second peak for a small scattering angle some particles are observed resulting from double collisions, causing a blurring of the Ar^+ peak. Moreover, we have observed that Ar^+ shows the strongest double scattering effects, Ar^{2+} less while Ar^{3+} and Ar^{4+} show only very weak broadening effects. Similar observations of double scattering effects for ejected Cu ions of different charge have been done[13].

This accounts for the increase in mean width k in fig. 2a for scattering angles smaller than 65° (angle of scattered particles with surface is $\varphi = 45°$ for this experiment). The monotonous increase in width for all charges for $\varphi > 65°$ is partly due to apparatus geometry, partly to spread in inelastic energy loss during the collision. These effects were considered in detail in

connection with measurements of the inelastic energy loss[3]). A careful analysis of peak formation and "tail" formation by double collisions has been given by Dahl *et al.*[16]). Also the effect of target temperature on double scattering has been considered.

The dependence of width on charge state for certain scattering angles, shows that application of a model which describes the charge changing processes as occurring after a single collision is not reliable for these scattering angles.

3.3. Results. Absolute numbers for the ion yield can be determined from formula (2a), by multiplying the width k by the intensity of a peak per unit primary beam intensity. As an example the intensity at the top of the scattered Ar^{2+} peak, divided by the primary beam (I/I_0) is given in fig. 2b as a function of scattering angle φ for the case of 60 keV Ar^+ on (100) Cu. The shape of this curve is representative for all projectile ion species, also at other primary energies or target orientations.

I/I_0 is measured relatively with the Bendix multiplier. Absolute calibration is performed by measuring with the Faraday cup at several scattering angles. The intensity initially increases with scattering angle, reaches a maximum and then always decreases monotonically. The low value of the ion intensity for small scattering angles is caused partly by neutralization as will be shown in sec. 6 and 7 of this paper and partly because of the smearing out of the peak by multiple collisions.

The decrease with higher scattering angles is a result of the dependence of the cross section for the production of scattered projectiles on scattering angle. For scattered Cu ions similar considerations apply.

Absolute yields for Ar and Cu ions scattered from a (100) surface of Cu, as calculated from the measurements by formula (2a) are given in fig. 4. A general feature of all curves of ion intensities is the rapid decrease for scattering angles where scattered ions move glancing along the surface. It can also be seen that the high charge states are most strongly influenced by the target: the top in the absolute yield curves appears at smaller scattering angles for lower charge states.

The intensities of scattered Cu ions also become very low near $\varphi = 90°$, because recoil particles scattered near 90° originate from very weak collisions, in which no strong ionizations occur.

We can compare the absolute yield curves with corresponding curves measured for the case of a gas target. Comparison of fig. 4 with fig. 2 of the previous paper clearly shows the large differences. We see that in the case of a solid target Ar^+ or Ar^{2+} have the highest intensities, while for a gas target Ar^{5+} or Ar^{6+} are most dominant in the corresponding region of scattering angles and primary energy. In the yield measurements of the Cu ions it is striking that in the whole accessible angular region $N(Cu^+) >$

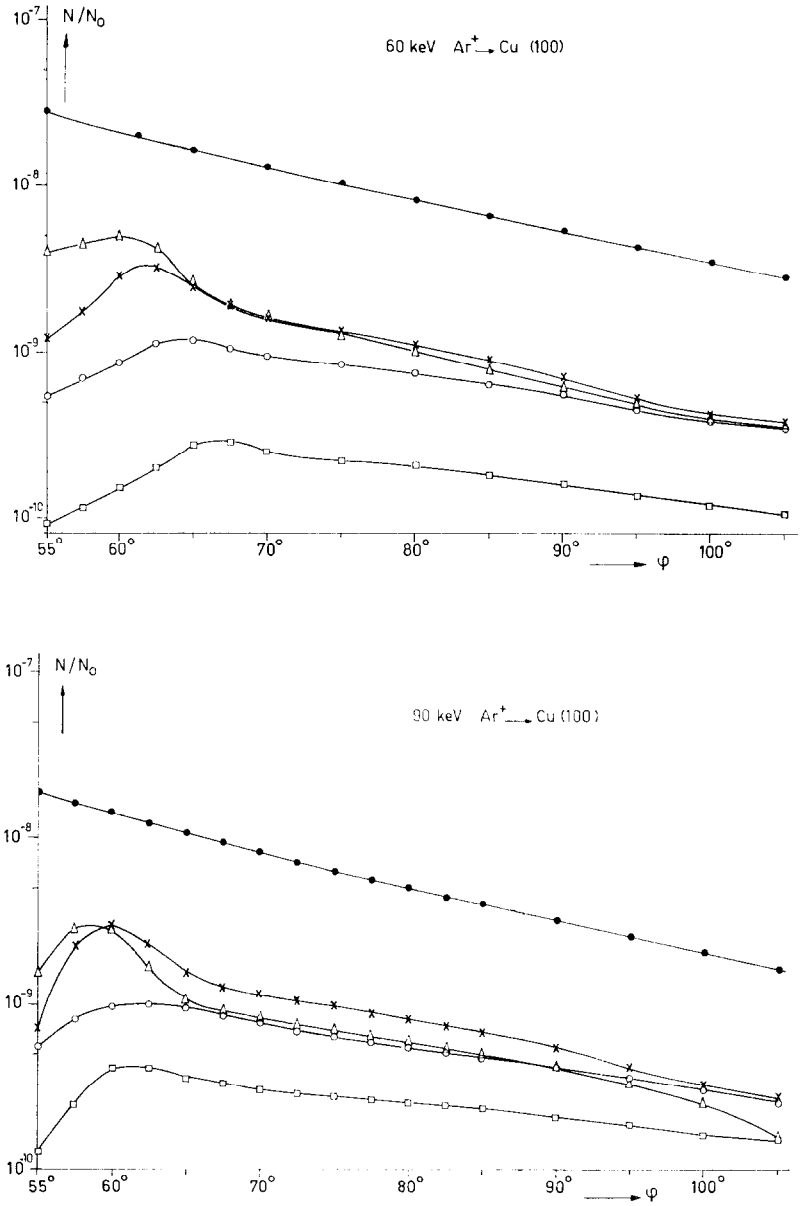

Fig. 4a. Number of Ar ions per incoming particle scattered into the solid angle of the analyzer as a function of scattering angle.

●: total number of scattered Ar particles estimated with the Bohr potential.

△: Ar^{+}, ×: Ar^{2+}, ○: Ar^{3+}, □: Ar^{4+}.

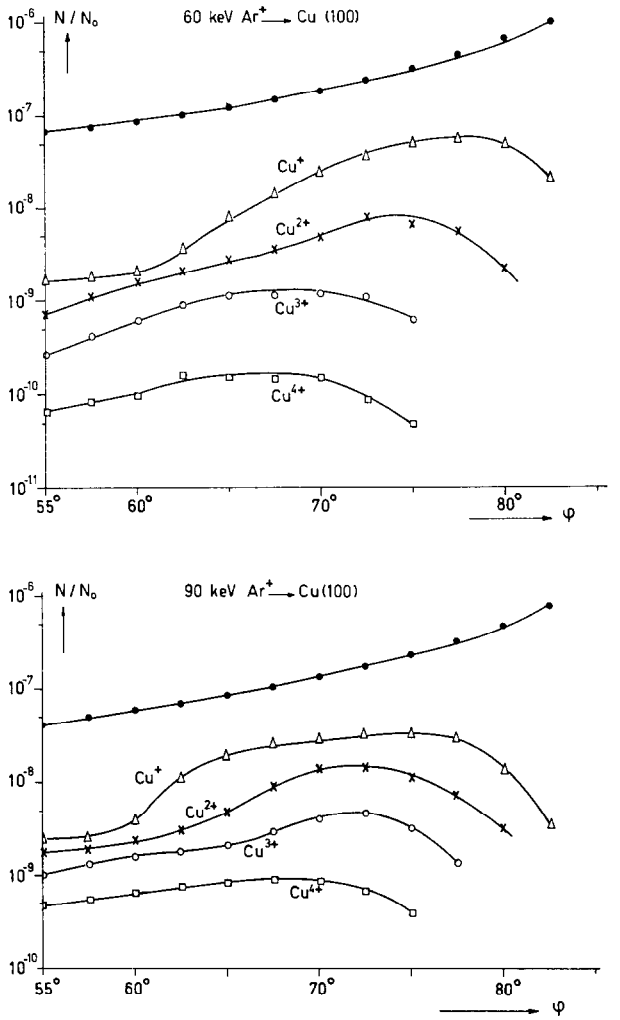

Fig. 4b. Number of Cu ions per incoming particle scattered into the analyzer *vs* scattering angle.

$> N(Cu^{2+}) > N(Cu^{3+}) > N(Cu^{4+})$, which is also a behaviour quite different from the gas target case.

4. *Determination of neutral scattered particle yield.* The yield of neutral particles resulting from binary collisions with surface atoms, as recorded by our multiplier, consists of a mixture of target and projectile particles. It is, however, very difficult to separate these two kinds of scattered atoms. There are indications that the energy spectrum of neutral scattered particles consists, like the energy spectrum of ions, of a background with superimposed peaks resulting from single collisions.

This information was obtained by performing a time of flight analysis of the scattered neutral particles[17]). This was done for the case of 40–90 keV Ar^+ ions on a (110) surface of Cu. The current of neutral particles compared with the total ion current indicates that ion neutralization is very important in the whole observable region of scattering angles when using a solid target. In the case of a gas target, neutral particles appear only near 0° (projectiles) and near 90° (recoils). The time of flight measurements even indicated that 50% of all singly scattered Cu particles are neutral for a primary energy of 60 keV and scattering angle of 70°. Ar neutrals from single collisions could not be observed as a result of insufficient resolution in the time of flight measurements.

Therefore we had to follow another procedure for a rough estimation of the neutrals.

Assuming a potential model, one can calculate the yield of scattered particles as a function of scattering angle. We used the screened Coulomb (Bohr) potential, which is known to give a good approximation for the considered collisions[18]):

$$V(r) = \frac{Z_1 Z_2}{4\pi\varepsilon_0 r} e^{-(r/a)}, \tag{3}$$

in which

$$a = \frac{a_0}{(Z_1^{\frac{2}{3}} + Z_2^{\frac{2}{3}})^{\frac{1}{2}}}; \qquad a_0 = 0.53 \text{ Å}.$$

Generally, the number of particles per incoming ion (N/N_0) scattered into the analyzer (solid angle $d\omega$) at scattering angle φ is given by:

$$\frac{N(\varphi)}{N_0} = \sigma(\varphi)\, n\, d\omega, \tag{4}$$

n is the number of atoms at the metal surface per unit surface perpendicular to the beam direction, $\sigma(\varphi)$ is the scattering cross section. Calculations of total scattered particle yield are also indicated in fig. 4; they were performed by eq. (4), using values of $\sigma(\varphi)$ as tabulated by Everhart *et al.*[19]).

In the discussion of the double scattering phenomenon (sec. 3.2) it was shown that many vacant lattice positions at the surface are created during ion bombardment. If a surface vacancy is created, an atom in the second layer of the crystal becomes "visible" to the beam.

A large part of the scattering products from collisions in the second layer can reach the surface by passing through the top layer of atoms. So, when computing the number of scattered particles we have to consider an effective density of scattering centers n_{eff}. It has been shown that n_{eff} approximates n (eq. (4)) closely for the case of bombardment of a (110) Cu single crystal surface[17]). The experimental total number of scattered parti-

cles was found to approximate the calculated number supposing an ideal undamaged crystal surface layer within 20%.

This means that for our case of a (100) single crystal, an estimation of the neutral particle component can be given by subtracting the measured ion current, summed over all charge states, from the yield as calculated by (4).

5. *Influence of crystal orientation on the ion charges.* 5.1. Time of flight variation. There are three experimental indications that the interaction of the scattered ions with the metal can be described with the time of flight near the surface as a parameter. We define the time of flight as the inverse of the velocity component of scattered particles which is perpendicular to the surface.

In the first place we observe in contrast to ion on gas target measurements[18]) the total scattered ion yield to decrease with primary energy for a fixed scattering angle. This is shown in table I. The lower primary energy results in a longer time of flight, increasing the neutralization probability.

Secondly we can compare the yield of ions from a (100) surface and a (110) surface.

Both surfaces are bombarded in {110} direction, which means that the same number of target atoms per unit surface perpendicular to the beam are present. The angle of emergence of the scattered beam with the (110) surface is $\varphi - 30°$, which is always larger than in the case of a (100) surface where this angle is $\varphi - 45°$. For the same scattering angle φ this means that particles leaving a (100) surface have a longer time of flight than particles leaving a (110) surface. Indeed it is observed that in the first case the ion yield is always lower than in the second one. An example is given in table I.

TABLE I

Measured ion yield relative to the total yield as calculated with the Bohr potential				
$\varphi = 70°$	$\left(\frac{N_{ion}}{N_{total}}\right)$Ar		$\left(\frac{N_{ion}}{N_{total}}\right)$Cu	
	60 keV	90 keV	60 keV	90 keV
(100)	0.35	0.38	0.16	0.34
(110)	0.50	0.63	0.42	0.48

The third indication of the influence of time of flight on the ion intensities is provided by the behaviour of the absolute ion yield curves *vs* scattering angle. For diminishing scattering angles, the intensities rapidly decrease (see fig. 4). However, these curves are not suitable to determine separately

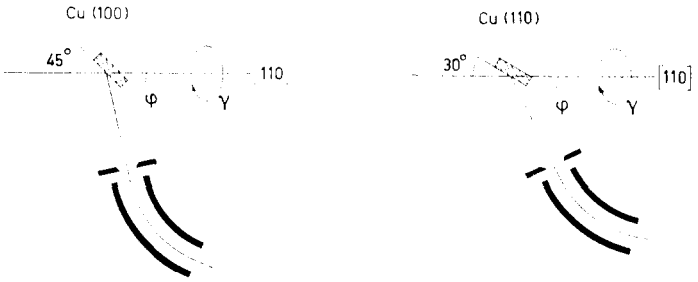

Fig. 5. Schematic view showing azimuthal rotations (γ) for the two bombarded Cu surfaces. Beam incidence in both cases is along a [110] direction.
For $\gamma = 0°$, a [010] axis is perpendicular to the incoming and scattered beam plane for the case of bombardment of the (100) surface and a $[1\bar{1}1]$ axis in case of the (110) surface.

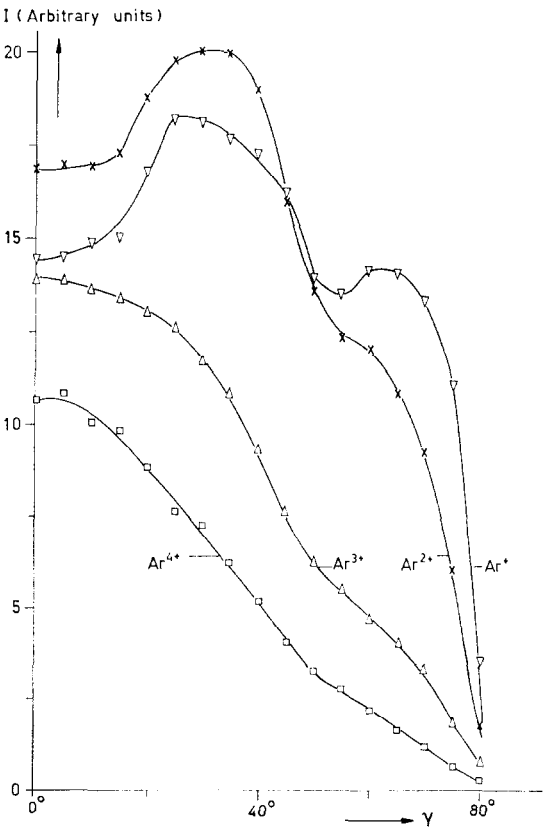

Fig. 6. Relative intensities of argon ions scattered from a Cu (100) surface as a function of azimuthal angle.
$\alpha = 45°$; $\varphi = 90°$.

the influence of the time of flight of scattered particles near a surface on their charge. The reason is that the total yield of particles is also a function of scattering angle φ, by the angular dependent cross section.

For this reason we performed the following experiment. With a fixed scattering angle we rotate the target around the direction of the primary beam (fig. 5), holding the angle between crystal and incoming beam at a fixed value. The parameters determining the collision with surface atoms (angle of incidence of primary ions, scattering angle) are not influenced by this rotation. The only thing which changes during this azimuthal rotation is the orientation of the surface with respect to the beam scattered into the analyzer. We denote the azimuthal angle by γ, $\gamma = 0°$ when the target surface is perpendicular to the plane of incoming and scattered beam. Increasing γ means increasing time of flight of scattered particles relative to surface.

We recorded scattered ion intensities as a function of γ, for several scattering angles and 3 primary energies. A typical example is given in fig. 6. One observes a general decrease in ion intensities for increasing time of flight. The higher charges decrease faster. However, superimposed upon this decreasing background, structure is observed. For $\gamma = 0°$ and $\gamma = 55°$ there are minima in the curves. This effect is strongest for the low charges and less pronounced for the higher charge states. These azimuthal curves were measured for scattering angles φ between 55° and 105°. The minima were present at all scattering angles. The minima are deeper for smaller φ. A remarkable feature is that the position of the minima is independent of the scattering angle. It does depend, however, on the crystal orientation of the surface; we observe minima at $\gamma = 0°$ and $\gamma = 55°$ for a (100) surface and at $\gamma = 0°$ and $\gamma = 35°$ for a (110) surface.

Furthermore, minima in curves of Ar ion intensities are much more pronounced than in curves of Cu ions.

The minima are more pronounced for increasing primary energies.

5.2. Change of azimuthal angle with fixed time of flight. When rotating the target over γ around the primary beam direction, the time of flight changes continuously. For this reason the structure in the azimuthal dependence curves of fig. 6 cannot be an effect of time of flight variation. To eliminate this time of flight effect, we measured ion intensities as a function of azimuthal angle only. Again the rotation is around the primary beam direction but now for perpendicular incidence of the beam; in this case the perpendicular velocity does not depend on γ. For scattering angles $> 90°$ scattered Ar ions can be detected. The result is shown in fig. 7 for three orientations of the target surface.

Strong structure appears again in the curves. Now the position of the minima can directly be correlated to the crystallographic orientation of the

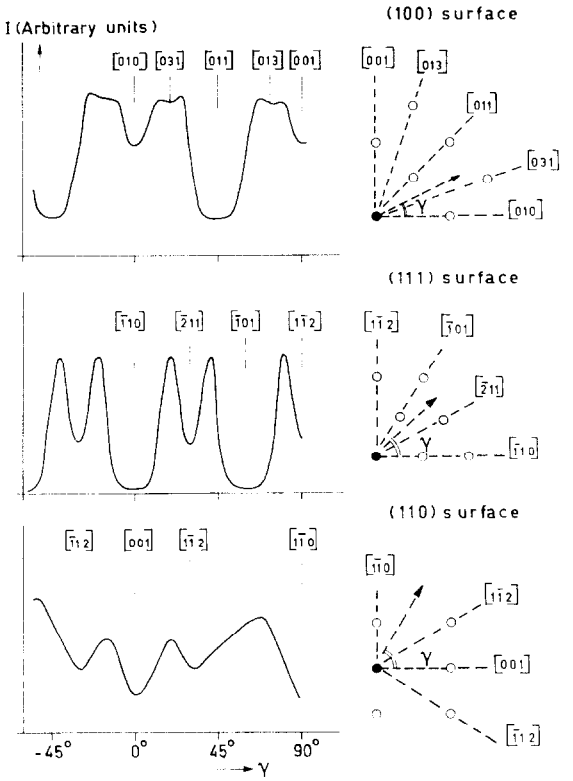

Fig. 7. Intensity of Ar^{2+} ions scattered under 105° from different Cu surfaces with normal incidence of 90 keV Ar^{+} ions as a function of azimuthal angle. At the right the surface is shown like the scattered particles "see" it. The arrow indicates the direction of scattered Ar^{2+} ions projected on the surface.

surfaces. This is observed most clearly in the case of the (100) surface (where identical structure repeats each 90°) and for the (111) surface (periodicity of 60°).

In fact, the curves in fig. 7 reveal that minima in the ion yield occur when the scattered particles pass a neighbour atom of the scattering center at a close distance. The nearest neighbours influence ion yields strongest. The ion intensity variation *vs* γ for perpendicular beam incidence is not the same for all charge states. In fig. 8 results are given for ions of different charges and for two primary energies.

It must be emphasized that perpendicular incidence of the ion beam and measuring the scattered-ion currents does not very well satisfy the conditions for studying charge changing processes of single scattered particles.

A normal incident beam on a (100) surface can "see" two atomlayers. In this case screening and blocking effects of the second by the first layer arise here. This is profoundly discussed elsewhere[16, 20].

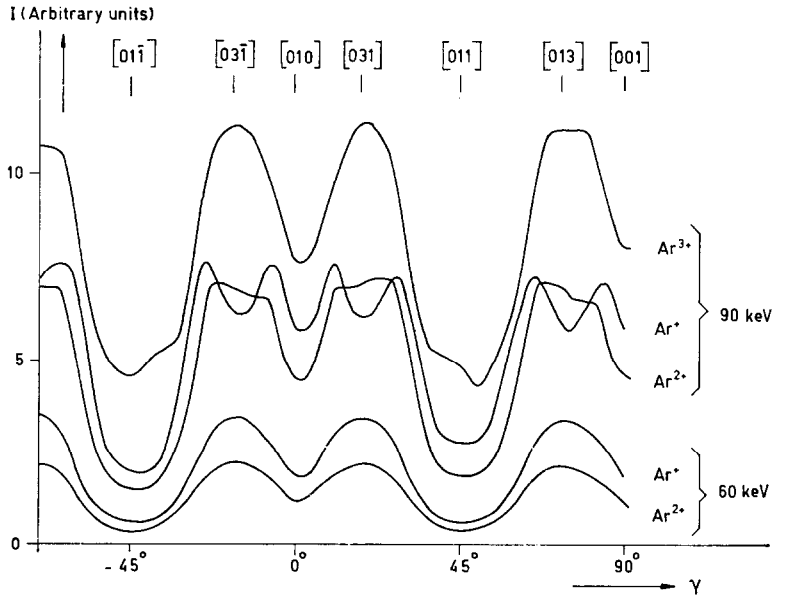

Fig. 8. Intensity of Ar ions of different charge scattered under 105° from a (100) Cu surface during normally incident bombardment as a function of γ for two primary energies.

5.3. Correlation of minima in ion yields and position of neighbour atoms. We shall determine the azimuthal angle γ for which the distance of scattered particles to neighbouring atoms is minimal.

Let $\boldsymbol{r}$ be the position vector of a surface lattice point in a coordinate system, in which the origin is the scattering center and in which the primary beam enters in the Y direction (fig. 9). Let $\boldsymbol{n}$ be the unit vector in the scattering direction (scattering angle φ).

The minimal distance d between a lattice point and a scattered beam

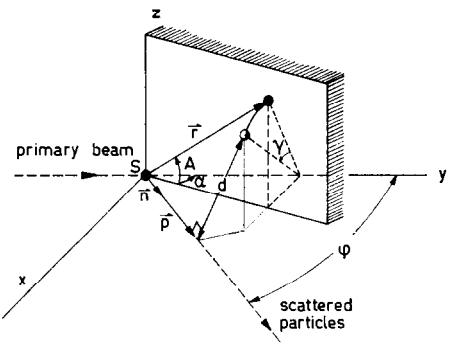

Fig. 9. Schematic representation of the crystal to illustrate the derivation of formula (7).

particle is found by projecting $\boldsymbol{r}$ on $\boldsymbol{n}$, let the projection be $\boldsymbol{p}$. When $|\boldsymbol{p}|$ is maximal, d is minimal.

$$|\boldsymbol{p}| = \boldsymbol{n}\cdot\boldsymbol{r} = (\sin\varphi, \cos\varphi, 0)\cdot(x, y, z) = x\sin\varphi + y\cos\varphi. \tag{5}$$

The condition for minimal d is:

$$\frac{\partial\,|\boldsymbol{p}|}{\partial\gamma} = \frac{\partial(x\sin\varphi + y\cos\varphi)}{\partial\gamma} = 0. \tag{6}$$

Because y is independent on γ (the target is rotated around the beam direction = Y axis) and φ is a constant, eq. (6) reduces to:

$$\partial x/\partial\gamma = 0. \tag{6a}$$

We can express x in the angles γ, A and α. A is the polar angle of the lattice atom in the surface plane, the scattering center S taken as origin. The angle of incidence of the primary beam on the surface is α.

Formula (6a) leads to the condition for γ, where d is minimal:

$$\tan\gamma = \tan A/\sin\alpha. \tag{7}$$

In case of perpendicular incidence of the ion beam ($\sin\alpha = 1$), the relation between γ for minimal distance and polar angle A is trivial; it is applied in fig. 7.

For the case of bombardment of the (100) surfaces ($\alpha = 45°$), we find by (7) the following values of γ corresponding with minimum d: $\gamma = 0°$, $\gamma = 25°$, $\gamma = 55°$.

Experimentally we find the 0° and 55° minimum always and the $\gamma = 25°$ minimum for small scattering angles. An example is given in fig. 6. The (110) surface ($\alpha = 30°$), leads to the following values: $\gamma = 0°$, 35°. In the experiments both minima are observed.

From formula (6a) it follows that the azimuthal angles, for which minima occur, are independent on the scattering angle φ.

Concluding we can state that minima in Ar ion yield occur when the distance between scattered particles and surface atoms near the scattering center is minimal. This influence is strongest for a) close neighbour atoms, b) small scattering angles and c) low charge states. For Cu ions in principle the same holds, but the effects are much weaker, in most cases only the $\gamma = 0°$ minimum is observed.

6. *Model for the collision and charge changing processes.* 6.1. Ionization and subsequent electron capture. We shall describe the ion formation during and after a collision of a projectile with a surface Cu atom in two phases.

The first part is the violent collision itself. During the collision a highly excited pseudomolecular complex is formed. This complex has a very short

lifetime ($< 10^{-16}$ s) and splits into two atoms, which separate in auto-ionizing states[21,22]). These states with internal energies of the order of 100 eV or more, also have a lifetime, which is of the order of the collision time. So during the separation of the molecule complex and immediately after it de-excitation of the collision partner takes place and ion formation occurs. Up to this stage of the collision, the ion formation, the collision is hardly influenced by the presence of the metal atoms and electrons. The only perturbing influence of the metal may be that the auto-ionization lifetimes even become shorter than in the case of a collision between free atoms. It seems reasonable to assume that any perturbation will tend to shorten the lifetime of an excited (molecular or atomic) state. The result is that we find immediately after the collision ions and neutrals in the same relative intensities as found in the case of primary ions hitting a free target atom[23]) in a gastarget.

The second part of the description is the electron capture of the ions formed in the violent collision. When an ion is at a close distance from the metal surface, transitions may occur, in which electrons from the metal tunnel to a vacant ionic level[5]).

The structure in the ion yields as a function of target orientation indicates that the metal surface cannot be described in the free-electron approximation. We have to include the variation of the potential energy of an electron in a crystal. A qualitative energy diagram of a solid surface is given in fig. 10. In it atomic levels are indicated, the deeper laying shells are associated to the atoms, the outer electrons may be in states which are spread out to a band extending through the whole crystal. When an ion comes close to the metal, electrons from the conduction band (or valence

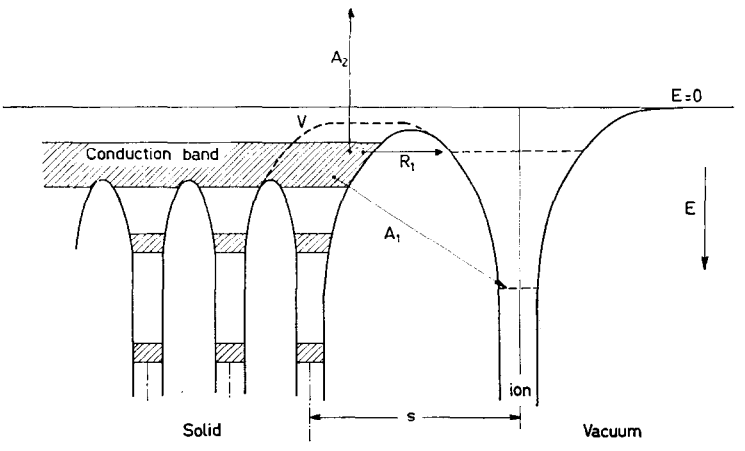

Fig. 10. Potential diagram of a metal and an ion at a distance s showing resonance processes (R_1) and Augerprocesses (A_1–A_2) leading to a decrease of ionic charge as well as to secondary electron emission if the available energy excess is large enough.

band in semi conductors and insulators) can tunnel through the surface potential barrier and neutralize the ion. If the top metal atom is removed, the potential barrier broadens and the probability for electron tunnelling decreases. Effectively the ion is at a larger distance from the metal surface.

Two types of electron transitions can be distinguished. In a resonance process there is no difference in potential energy between the initial (metal) state of the electron and the final (atomic) state. It is indicated in fig. 10 by R_1.

An Auger process is a two-electron process, during which a (metal) electron tunnels to an energetically deeper laying vacant state of the ion; the energy difference is transferred to a second metal electron which may escape and appear as a secondary electron (electrons A_1 and A_2 respectively in fig. 10). In case of highly charged ions near a metal surface Auger processes will occur. This process of ion neutralization is very analogous to the mechanism of potential ejection of electrons[5]). Hagstrum showed that these Auger processes and eventually, the resonance processes, have a very high probability when the distance metal-ion is of the order of a few Å.

6.2. Differential equations for charge exchange. The probability for these electron transitions is distance dependent and also a function of the potential energy of the ionic state which interacts with the metal. We will make some approximations.

1) For a fixed distance the probability for an Auger process in which an ion changes its charge from n to $n - 1$ is only a function of the energy difference between the ground states of the n times and $n - 1$ times charged ion, i.e. a function of the n-th ionization energy.

This means that we approximate the energy of an excited n-times charged ion by the ground state energy, although the statistical mechanism for ionization during the first violent collision as worked out in the previous paper[23]), indicates that a high degree of excitation is left in the scattered particles.

2) The dependence of transition probability on distance does not contain dependence on energy levels of interacting electrons.

3) Changing of charge from n to $n - 1$ is much more probable than from n to $n - i$, with $1 < i \leq n$. So we suppose that neutralization of an n times charged ion takes place in n successive one electron steps.

4) We do not consider electron loss. From the diagram of fig. 10 one sees that ionization by Auger effect is energetically impossible.

Let the probability that an ion with charge n moving at a distance s from the metal, changes its charge by electron capture into $(n - 1)$ be:

$$W_n(s).$$

The final charge-state distribution which is measured in the analyzer is a result of series of capture processes near the surface where the initial

(gaslike) charge state distribution ($s = 0$) changes continuously. The change of the number of ions with charge n per unit time is caused by charge changing of $n \to n - 1$, which decreases the yield of n times charged ions and on the other hand by transitions from $n + 1 \to n$ which increase the yield. Furthermore it is clear that at any moment the rate of change due to the process ($n \to n - 1$) is proportional to the number of ions with charge n. These statements are mathematically formulated in the following set of coupled differential equations:

$$\mathrm{d}P_n(s) = \{- W_n(s)\, P_n(s) + W_{n+1}(s)\, P_{n+1}(s)\}\, \mathrm{d}t. \tag{8}$$

$P_n(s)$ is the fraction of n times charged ions at a distance s for a fixed scattering angle. If we separate $W_n(s)$ in a distance dependent and charge dependent part, which is possible according to approximation 2):

$$W_n(s) = A_n\, f(s) \tag{9}$$

the set (8) can be solved analytically.

Investigations on secondary electron emission[5]) and also theoretical estimations of the transition matrix elements[24, 25]) show that the distance dependence can be approximated by an exponential function

$$f(s) = \mathrm{e}^{-as}. \tag{10}$$

6.3. Solution of the differential equations. Experimentally we find in the case of collision in a gas that for the used region of primary energies and scattering angles the highest charge number observed is 8. Since by the interaction of the ions with the surface the charge can only decrease we need to consider 9 equations, $n = 0, \ldots, 8$ in formula (9), and use $P_9 = 0$.

Starting with $n = 8$ the equations (9) can be solved analytically in steps.

$$\mathrm{d}P_8(s) = -W_8(s)\, P_8(s)\, \mathrm{d}t.$$

We substitute (9) and write

$$\mathrm{d}t = \frac{\mathrm{d}t}{\mathrm{d}s}\, \mathrm{d}s.$$

For the case of a particle moving with a certain velocity along a plane surface $\mathrm{d}t/\mathrm{d}s$ means the inverse of the velocity component perpendicular to the surface ($v_\perp$). Now the solution follows immediately:

$$P_8(s) = P_8(0) \exp\left[- A_8 \int_0^s f(x)\, \frac{\mathrm{d}t}{\mathrm{d}x}\, \mathrm{d}x\right]. \tag{11}$$

P_8 decreases exponentially from its initial value $P_8(0)$. We observe that

only the integrated distance-dependent part of transition probability (with a weight factor accounting for the particle velocity) appears in the solution. Let $F(s)$ be equal to

$$\int_0^s f(x) \frac{\mathrm{d}t}{\mathrm{d}x} \mathrm{d}x,$$

then (10) can be substituted in the next differential equation ($n = 7$). The solution for P_7 is:

$$P_7(s) = \frac{A_8}{A_7 - A_8} P_8(0)\, \mathrm{e}^{-A_8 F(s)} + \left(P_7(0) - \frac{A_8}{A_7 - A_8} P_8(0) \right) \mathrm{e}^{-A_7 F(s)}. \tag{12}$$

Besides the initial intensity of charge 7 also the effect of contributions of P_8 appears in this equation. The general solution is

$$\begin{aligned} P_8(s) &= P_8(0)\, \mathrm{e}^{-A_8 F(s)}, \\ P_k(s) &= P_k(0)\, \mathrm{e}^{-A_k F(s)} + \sum_{m=1}^{8-k} (-1)^m P_{k+m}(0) \times \\ &\quad \times \prod_{l=1}^{m} A_{k+l} \sum_{j=0}^{m} \frac{\mathrm{e}^{-A_{k+j} F(s)}}{\prod_{\substack{i=0 \\ i \neq j}}^{m} (A_{k+j} - A_{k+i} + \delta_{ij})}, \\ &\qquad\qquad (k = 1, \ldots, 7) \\ P_0(s) &= 1 - \sum_{i=1}^{8} P_i(s). \end{aligned} \tag{13}$$

P_0 is simply found by the conservation of the total number of particles during interaction with the surface.

As we are using a target of macroscopic size, the resulting charge state distribution, which is observed in our analyzer can be obtained from (13) putting $s = \infty$. Numerical values of P_n can be obtained by substituting values for A_n. However, the transition probability for Auger processes involving multiply charged ions is not known. Therefore we make an assumption about the behaviour of A_n on the state of charge n. We put

$$A_n = A(E_n)^p. \tag{14}$$

A and p are constants which we have to determine, and E_n is the ionization potential of the n-th bound electron.

By (14) we state that the probability for the Auger process is a monotonic function of the energy which is liberated by capture of an electron in an n times charged ion. For an ideally flat target surface plane we have,

$$F(\infty) = \int_0^\infty \frac{\mathrm{d}t}{\mathrm{d}s} f(s)\, \mathrm{d}s = \frac{1}{v_\perp} \int_0^\infty f(s)\, \mathrm{d}s = \frac{I}{v_\perp} \tag{15}$$

in which I is the integrated distance-dependent part of transition probability and $v_\perp$ the velocity component of the ion perpendicular to the surface. The $P_n(0)$ values we determine from our scattering experiments of Ar ions in a Cu vapour target. In other words, now we use the first part of our description of the collision process, which states that this violent collision is an undisturbed binary collision (see 6.1). *I.e.* using the gas target values of P_n, enables us to give numerical solutions for the set (8). Of course one has to take corresponding scattering angles and primary energies. We plot the $P_n(\infty)$ functions *vs* the parameter $\tau = AI/v_\perp$. The foregoing discussion showed that all solutions can be expressed in terms of τ. We can do this for different p values (see eq. (14)).

The results for $p = 1$, scattering angle $\varphi = 105°$, and primary energy of 90 keV is given in fig. 12 for scattered Ar ions.

After an initial increase because of the contribution of higher charge states, all P_n functions (for $n > 0$) decrease, for larger τ only low charges result and finally also Ar^{2+} and Ar^+ do not survive the neutralizing influence of the surface and become neutral.

For high velocity particles or for small transition probability many particles with high charge states are observed. Both cases are expressed by small τ.

7. *Comparison of measured and calculated ion intensities.* 7.1. Ion intensities *vs* scattering angle φ. The structure of a surface during ion bombardment is such, that we must distinguish between two types of charge changing processes. In the first place we have to consider charge changing of ions scattered from a metal atom with a neighbouring atom being closely located to the orbit of the scattered ion. Secondly also scattering processes from atoms with one or more vacancies surrounding the collision center occur, which is equivalent to scattering from atoms situated at the edge of a step or ridge in the surface.

From fig. 10 the importance of a near neighbour on the electron transition probability can be estimated. The potential wall between metal and ion is indicated by a solid line. When the top surface atom is not present, the potential wall is considerably broader (it is indicated by V and a dotted line in fig. 10). It is generally assumed[5,24,25]) that the transition probability is a rapidly varying function of distance s (an exponential dependence has been suggested). For this reason the two types of processes will have quite different probabilities and will result in different relative ion intensities.

The measured ion intensities are formed by a superposition of contributions from both processes. Scattering from an atom with neighbours will lead to formation of neutrals and low charges. In fig. 11 the value of the integrated transition probability for this process is schematically indicated

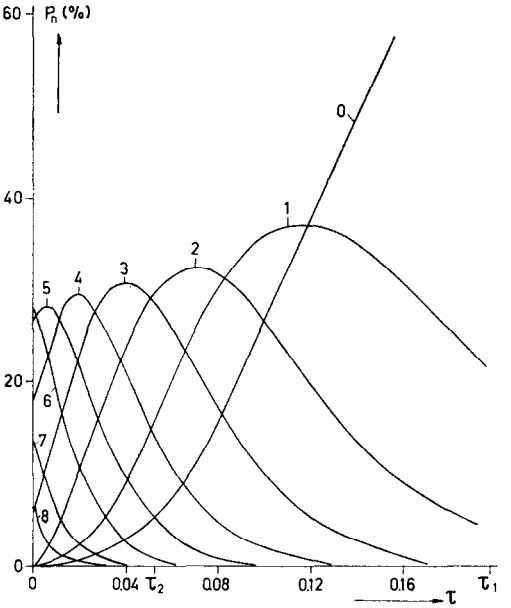

Fig. 11. Solution of the set of equations (8) as a function of τ which is the integrated transition probability over the perpendicular velocity ($\tau = AI/v_\perp$).

by τ_1. Highly charged ions will come predominantly from atoms without neighbour (τ_2 in fig. 11). We have restricted ourselves to a description of the second process, because the neutral contribution in the case of ion-surface scattering is known with insufficient accuracy.

As the fraction of surface atoms without neighbour is not known, we shall relate measured *relative* ion intensities to the calculations by the following procedure. In a set of curves of ion intensity *vs* integrated transition probability like in fig. 11 we determine the value of τ for which the relative ion intensities as calculated approximate the measured ones closest. This is only done for the charges 2, 3 and 4 for the reasons mentioned above and for a primary energy of 90 keV and scattering angle of 105°. For these experimental conditions no double scattering effects occur, which eventually could disturb the picture.

Several p values in expression (13) were tried; from $p = 0$ which means that the transition probability is independent on ionization energy, to $p = 3$. A variation of p profoundly influences the relative values of the intensities for each τ, which makes the choice significant. Only the value of $p = 1$ resulted in the possibility of finding a value of τ, where the calculated data fitted the experiment.

This procedure determines the integrated transition probability very sensitively as is shown in table II. Once we have obtained a value of τ for one scattering angle by comparison of theory and experiment, we can

TABLE II

Measured relative ion intensities compared with calculated relative ion intensities for different values of τ

	experiment	calculated		
		$\tau = 0.046$	$\tau = 0.052$	$\tau = 0.058$
Ar^{3+}/Ar^{2+}	0.93	1.07	0.93	0.83
Ar^{4+}/Ar^{2+}	0.53	0.62	0.44	0.36

find τ for other scattering angles and energies and thus obtain theoretical $P_n(\varphi)$ functions.

At $\varphi = 105°$, $E_0 = 90$ keV we have determined $\tau_2 = 5.2 \times 10^{-2}$ to describe the experimental values (see table II). From this value we determine τ as a function of scattering angle. Only $v_\perp$, which is known, changes with φ:

$$v_\perp = v_0 \sin(\varphi - \alpha). \tag{16}$$

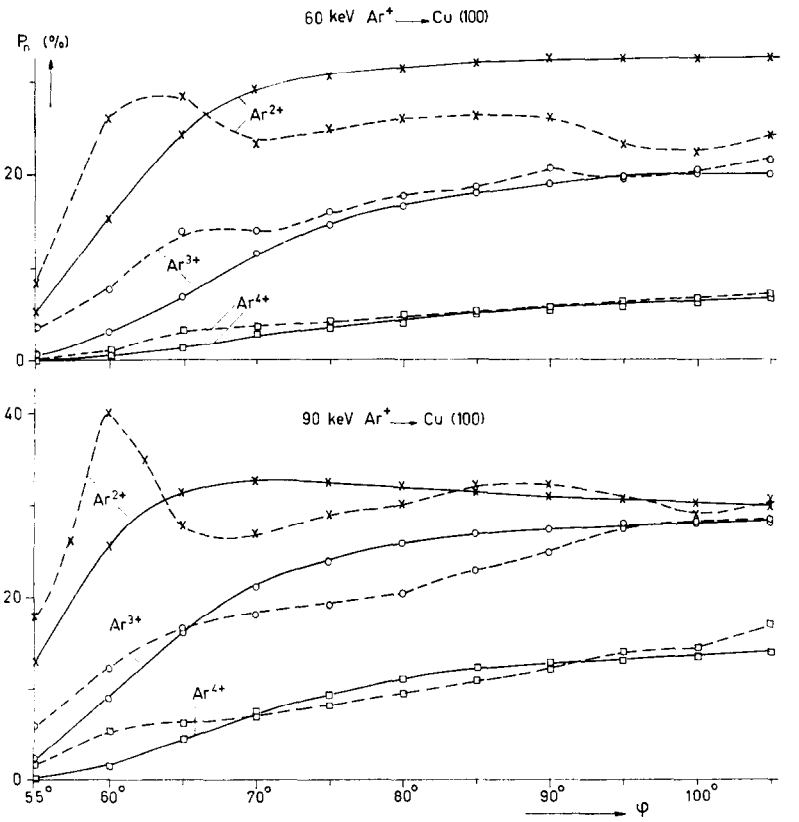

Fig. 12. Experimental and calculated curves of relative ion yields as a function of scattering angle φ.
Experimental curves are dashed.

The transition probability obviously does not depend on φ (remember that τ is the integrated transition probability divided by the perpendicular velocity component). Also the differential equations (8) can be solved for each scattering angle. To accomplish this, we substituted the values of the relative ion intensities which were measured for a gas target[23]) as initial conditions in the solutions (12) of the differential equations. Taking the values for P_n computed in this way for each scattering angle φ for the relevant τ results in the theoretical $P_n(\varphi)$ functions. We compare them only with the measured intensities of Ar^{2+}, Ar^{3+} and Ar^{4+}.

Also P_n values for $E_0 = 60$ keV can be calculated now without further adaption to experimental values, because only $v_\perp$ and the initial conditions in the differential equations change with primary energy and not the value of the integrated transition probability. Results are presented in fig. 12.

Measurements of scattered ion intensities from a (110) surface of Cu are also available. Assuming that the transition probability does not depend strongly on the surface orientation, also theoretical curves can be predicted, with the help of the value of τ as determined for the (100) surface. Again only $v_\perp$ changes in going from a (110) to a (100) surface, because of the

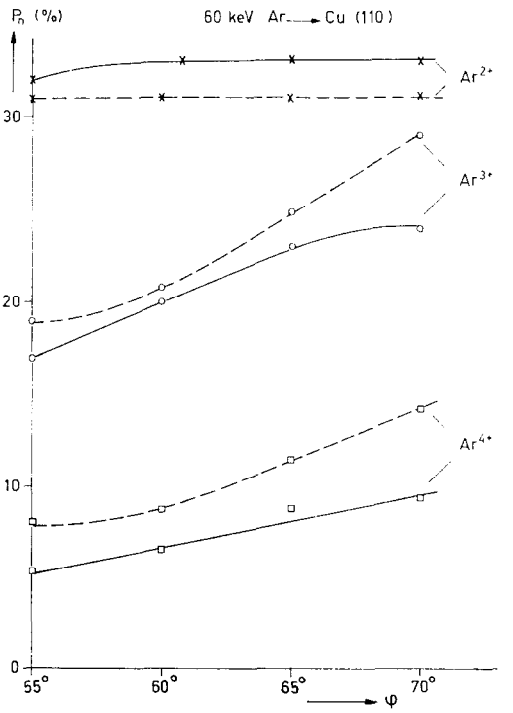

Fig. 13. Comparison of calculated and measured relative ion yields from a (110) surface of Cu. (Dashed curves experimental.)

change in angle between ion beam and surface. Calculated values approximate the experimental values closely (fig. 13).

It is, however, doubtful whether $v_\perp$ is a good parameter for the description of ion intensities for small scattering angles. When scattered particles emerge under an angle smaller than 20° with the surface, microstructure and double collisions become important disturbing effects. In fig. 12 we observe indeed that for $\varphi < 70°$ the calculated and experimental curves deviate. More evidence for this effect is given by comparison of results of calculation and experiment for scattered Cu ions. Here also the description is no more valid for $\varphi < 70°$. Calculations show that in the whole measured angular region the ion intensity curves for different charge states do not cross and resemble the experimental curves (fig. 4) in general shape, but for $\varphi < 70°$ relative intensities are incorrectly predicted. Cu^{3+} and Cu^{4+} are only present for $\varphi < 75°$, therefore the comparison between theory and experiment can only be performed in a very limited angular region. Results for $\varphi = 70°$ are given in table III.

TABLE III

Intensity of Cu ions normalized on the Cu^{4+} intensity				
$\varphi = 70°$		Cu^{2+}	Cu^{3+}	Cu^{4+}
$E_0 = 60$ keV	exp.	30	8	1
	calc.	32	8	1
$E_0 = 90$ keV	exp.	15	5	1
	calc.	10	4.5	1

Like in the Ar case, we have found for these Cu ions a value of τ for the 90 keV case and used it to determine relative intensities in the 60 keV case. We see that also for Cu the significant change in the relative ion intensities with primary energy can be described by the concept of change of perpendicular velocity. We have determined a value of τ, which now can be expressed in a (compare sec. 6.2.)

$$\tau = \frac{AI}{v_\perp} = \frac{A}{v_\perp} \int_0^\infty f(s)\, \mathrm{d}s = \frac{A}{a v_\perp}. \tag{17}$$

In the case of charge exchange of Ar ions, for $E_0 = 90$ keV, $\varphi = 105°$ we found: $\tau = 5.2 \times 10^{-2}$.

From ref. 5 we take $a = 2$ Å^{-1} as a reasonable value. With $v_\perp = 2.3 \times 10^7$ cm/s, the result is:

$$A = 2.4 \times 10^{14}\ \mathrm{s}^{-1}.$$

The transition probability $W_n(s)$ can be given now with the help of eqs.

(9) and (14):

$$W_n^{\mathrm{Ar}}(s) = 2.4 \times 10^{14} (E_n)_{\mathrm{Ar}} \, \mathrm{e}^{-2s}, \tag{18}$$

s is expressed in Å and E_n in eV.

The case of charge changing of Cu ions near a Cu surface leads to:

$$W_n^{\mathrm{Cu}}(s) = 1.1 \times 10^{14} (E_n)_{\mathrm{Cu}} \, \mathrm{e}^{-2s}. \tag{19}$$

The relevant ionization energies may be taken from the tables by Lotz[27]).

These results indicate that the Auger processes at a distance of a few Å are rather fast processes. For instance for $n = 3$ and $s = 2$ Å, we find $W_3^{\mathrm{Ar}} = 1.3 \times 10^{15}\ \mathrm{s}^{-1}$. The absolute values for the transition probability obtained in this way are in agreement with values determined by measurements and calculations of potential secondary emission (see for instance table X in ref. 5).

7.2. Ion intensities *vs* azimuthal angle γ. In general the variation of ion yield with γ is simply caused by the change in $v_\perp$ of scattering products when rotating the crystal. The experimental curves of fig. 6 can directly be compared with the calculated curves of which fig. 11 is an example, after determining the relation between $v_\perp$ and γ:

$$v_\perp = v_0(\sin\varphi \cos\alpha \cos\gamma - \cos\varphi \sin\alpha). \tag{20}$$

Like in sec. 7.1 this can best be done for curves of Ar^{3+} and Ar^{4+}, because the structure in the curves for Ar^{+} and Ar^{2+} cannot be explained only by the $v_\perp$ variation. Comparison of measured and calculated $I(\gamma)$ curves can be done by taking the value of τ as determined in the previous section where all discussions applied to cases with $\gamma = 0$.

The result is that for small values of γ, experiment and theory coincide within 20%, for large γ where scattered particles emerge under a small angle with the surface, strong deviations occur. This points in the same direction as the deviation for small φ in sec. 7.1. Again our conclusion is, that for small angles with the surface, $v_\perp$ is not an appropriate parameter to describe the charge changing.

To explain the fact that structure appears in the $I(\gamma)$ curves for Ar^{+} and Ar^{2+} (fig. 7) we have to consider scattering from atoms with a close neighbour atom (first process in sec. 7.1). We have already indicated that the result of such collisions is that predominantly singly charged and neutral particles are formed. The effect of turning the crystal in such a way that a neighbour atom comes close to the path of a scattered beam particle is to increase the transition probability $W(s)$, as can be seen from the potential-energy diagram fig. 10. The result in terms of the solution of the differential equations is that the value of τ_1, (fig. 11), increases when a neighbour atom comes close. This leads to an increase in the neutral-particle yield and a

minimum in the ion yield for the *low* charge states, as experimentally observed.

8. *Discussion and conclusions.* We have applied a model which considers a violent collision of a projectile ion with a surface atom as an undisturbed 2-body collision followed by an electron capture process of scattered ions, to describe the observed relative ion intensities. The measured ion yields from a solid surface can be related to the ion yield in a gas collision via a set of differential equations, describing the charge changing process. We observed that this description which relates the observed ion intensities with time of flight near the surface (or $v_\perp$) is valid for cases where scattered particles leave the surface at not too small angles. This follows from the behaviour of ion intensity as a function of scattering angle, azimuthal angle, primary energy and target orientation.

Evidence from measurements of double scattering and also of effects of crystal orientation on ion yield leads to the interpretation of results in terms of two types of collisions, one from an atom without neighbour and another from atoms with close neighbours. This distinction into two types of collisions and its result on the charge state has also been considered by Dahl *et al.*[16]).

A serious limitation of the experiments is that we are not able to determine precisely the scattered neutral particle yield. Therefore we cannot determine the relative importance of the two types of scattering processes. The distinction in two types, however, permits a natural explanation for the observed correlation between double scattering effects and charge state. We have seen (sec. 7.1) that collisions with atoms with a neighbour result in low charge states, which explains the fact that double-scattering effects are most strongly observed on singly charged scattering products (see sec. 3.2).

The used potential model of the metal surface which is a combination of atomic and metallic electron states, qualitatively shows the increased probability for electron transitions when a surface atom is near the scattered ion. In this case the potential barrier, through which the electrons have to tunnel is relatively narrow. In order to test the significance of the conduction band for these processes we have performed some experiments on the relative ion intensities in case of scattering from a Ge surface. For corresponding scattering angles we found no significant differences in charge state population between scattering from Ge or from Cu. This observation is in accordance with earlier measurements on the charge state of scattering products from Cu_2O, which also showed no difference from the case of a Cu target[2]).

The conclusion is, that as in the potential-electron ejection[26]) we do not need free electrons for the electron capture processes. The only important factors are the presence of electrons in suitable energy states and the density

of states; they may be conduction electrons, electrons from the valence band in semiconductors and insulators or even electrons associated with lattice atoms.

Acknowledgements. The authors thank Professor J. Kistemaker, Dr. C. Snoek and Dr. D. Onderdelinden for their continuous interest in the work and for many valuable discussions.

Much credit is due to S. Doorn and H. H. Roukens for their help in the experimental work.

Computer calculations were performed with the X8 computer of the Mathematisch Centrum, Amsterdam.

This work is part of the research program of the Stichting voor Fundamenteel Onderzoek der Materie (Foundation for Fundamental Research on Matter) and was made possible by financial support from the Nederlandse Organisatie voor Zuiver-Wetenschappelijk Onderzoek (Netherlands Organization for the Advancement of Pure Research).

REFERENCES

1) Snoek, C. and Kistemaker, J., Adv. Electronic and Electron Physics, Acad. Press (New York, 1965) p. 67.
2) Datz, S. and Snoek, C., Phys. Rev. **134** (1964) A 347.
3) Snoek, C., Van der Weg, W. F., Geballe, R. and Rol, P. K., Physica **35** (1967) 1.
4) Snoek, C., Van der Weg, W. F., Geballe, R. and Rol, P. K., Proc. VIIth Int. Conf. on Phenomena in Ionized Gases, Belgrade, 1965, p. 145.
5) Hagstrum, H. D., Phys. Rev. **96** (1954) 336.
6) Snoek, C., thesis, Amsterdam, 1966, p. 38.
7) Snouse, T. W. and Haughney, L. C., J. appl. Phys. **37** (1966) 700.
8) Onderdelinden, D., thesis, Leiden, 1968, p. 30.
9) Nelson, R. S., Phil. Mag. **9** (1964) 343.
10) See for instance Carter, G. and Colligon, J. S., Ion Bombardment of Solids, Heinemann (London, 1968) Ch. 4.
11) Mashkova, E. S., Molchanov, V. A., Parilis, E. S. and Turaev, N. Yu., Soviet Physics-Doklady, Engl. Transl. **11** (1966) 52.
12) Parilis, E. S., Proc. VIIth Int. Conf. on Phenomena in Ionized Gases, Belgrade, 1965, p. 129.
13) Van der Weg, W. F. and Bierman, D. J., Physica **38** (1968) 406.
14) Farnsworth, H. E. and Hayek, K., Surface Sci. **8** (1967) 35.
15) Lyon, H. B. and Somorjai, G. A., J. chem. Phys. **46** (1967) 2539.
16) Dahl, P. and Sandager, N., Surface Sci. **14** (1969) 305.
17) Snoek, C., thesis, Amsterdam, 1966, p. 46.
18) Fuls, E. N., Jones, P. R., Ziemba, F. P. and Everhart, E., Phys. Rev. **107** (1957) 704.
19) Everhart, E., Stone, G. and Carbone, R. J., Phys. Rev. **99** (1955) 1287.
20) Yurasova, V. E., Shulga, V. I. and Karpuzov, D. S., Canad. J. Phys. **46** (1968) 759.
21) Everhart, E. and Kessel, Q. C., Phys. Rev. **146** (1966) 27.
22) Lichten, W., Phys. Rev. **164** (1967) 131.

23) Van der Weg, W. F., Bierman, D. J. and Onderdelinden, D., preceding paper, Physica **44** (1969) 161.
24) Sternberg, D., Thesis, Columbia University, 1957.
25) Gadzuk, J. W., Surface Science **6** (1967) 133, ibid. **6** (1967) 159.
26) Hagstrum, H. D., Phys. Rev. **122** (1961) 83.
27) Lotz, W., J.O.S.A. **57** (1967) 873.